



Highly efficient ultrasonic-assisted removal of methylene blue from aqueous media by magnetic mesoporous silica: experimental design methodology, kinetic and equilibrium studies

Somaye Nourozi, Rouholah Zare-Dorabei*

Research Laboratory of Spectrometry & Micro and Nano Extraction, Department of Chemistry, Iran University of Science and Technology, Tehran 16846-13114, Iran, Tel. +98 21 77240646; Fax: +98 21 77491204; emails: zaredorabei@iust.ac.ir (R. Zare-Dorabei), somayenoroozi37@gmail.com (S. Nourozi)

Received 1 August 2016; Accepted 14 July 2017

ABSTRACT

In the present study, a magnetic mesoporous silica (SBA-15-HESI-Fe₃O₄) was used as adsorbent for removal of methylene blue from aqueous solution. Ultrasound irradiation was employed to accelerate chemical process. In this study, influence of different parameters such as pH, initial dye concentration (mg L⁻¹), adsorbent dose (mg) and sonication time (min) on adsorption process were investigated. Central composite design was performed to obtain the optimum levels of parameters using response surface methodology and to investigate the possible interaction between variables. Under the best condition (pH = 9, dye concentration = 25 mg L⁻¹, adsorbent dose = 10 mg and sonication time = 2.2 min), the experimental equilibrium data were fitted to various isotherm models such as Langmuir, Freundlich and Tempkin. The results revealed the suitability and applicability of the Langmuir model. Different kinetic models including pseudo-first-order and pseudo-second-order were assessed and it was found that removal process followed pseudo-second-order kinetics. Ultrasonic power had important role in shortening the adsorption time of ions by enhancing the dispersion of adsorbent in solution. Overall, the as-synthesized adsorbent showed high adsorbent capacity ($q_e = 172.3 \text{ mg g}^{-1}$) for successful dye uptake on the real wastewaters in a short time (2.2 min).

Keywords: Methylene blue; Magnetic mesoporous adsorbent; Wastewater; Sonication; Experimental design; Kinetic and equilibrium isotherms

1. Introduction

Dyes are widely used in different industries such as paper, textile, food and related industries. As the discharge of this aromatic and heteroaromatic compounds into the aqueous media will generate potential risks for human and animal health, dye removal from industrial effluents is an urgent need [1–5]. Methylene blue (MB) is a common carcinogenic colored material used for coloring paper, dyeing wools, cotton and so on [6]. In recent years, various technologies including flocculation, coagulation, precipitation, membrane filtration, electrochemical techniques and adsorption are developed for treatment of dyes from wastewaters.

Among them adsorption has a great demand due to its high efficiency, capacity and large-scale ability of regenerable adsorbents [7–15]. Nanoadsorbents possess attractive properties such as high number of reactive atoms and large number of vacant reactive surface sites for interaction with different reactive groups of target compound [16,17]. The experimental design technique is a faster, more efficient and cost-effective method compared with the conventional methods of studying a process that can be provided simultaneous optimization of several affecting factors with consideration of their possible interactions. The central composite design (CCD) is one kind of multivariate-based methods making a better prediction of output response in less number of experiments and minimum errors [18,19]. Recently, functionalized mesoporous materials, possessing high surface area and

* Corresponding author.

tenability of the surface functionality, have gained increasing importance in their use as adsorbents [20–24].

In this study, a modified SBA-15 with covalently bonded N-(2-hydroxy ethyl) salicylaldimine Schiff base as a ligand (SBA-15-HESI) composited with iron oxide nanoparticles was employed as an adsorbent for the removal of MB from aqueous solution [25]. Experimental design method was applied instead of one factor at a time. All conventional parameters, except the parameters under study, were controlled, so allowed no interactions and required a large number of experiments to find the optimum conditions. Experimental design method is faster, more efficient and low-cost technique that provides simultaneous optimization of several variables with their interactions. In this case, the interactions of the parameters will be described. Also, ultrasonic irradiation was used to increase the kinetics of the adsorption process. Moreover, the present adsorbent is powerful and cost-effective.

Ultrasound irradiation was used for ultrasound-assisted dye adsorption. The power of ultrasound irradiation accelerates chemical process [26–29]. SBA-15-HESI-Fe₃O₄ nanocomposite was synthesized and characterized by different techniques such as scanning electron microscopy (SEM), X-ray diffraction (XRD) and Brunauer, Emmett and Teller (BET) analysis. CCD was applied for the optimization of effective variables in absorption efficiency such as pH of solution, dye initial concentration (mg L⁻¹), adsorbent dose (mg) and sonicating time (min). The kinetic and equilibrium isotherm of adsorption process were studied for investigating its mechanism. Removal performance of adsorbent on some real waters was also examined.

2. Materials and methods

2.1. Materials and instruments

All chemicals with the highest purity were purchased from Merck (Darmstadt, Germany). An ultrasound bath (Elmasonic, Germany) at 60 Hz of frequency and 500 W of power were used for shaking and dispersing solutions. pH measurements were done using pH meter model 691 (Metrohm, Switzerland). UV–Vis spectrophotometer model T80+ (PG Instruments, China) was used to analyze MB concentration at the maximum wavelength of 664 nm. A magnet with power of 1 tesla was used to separate the adsorbent from solution.

2.2. Synthesis of SBA-15-HESI-Fe₃O₄ nanocomposite

SBA-15-HESI-Fe₃O₄ was prepared by the hydrothermal method [18,25] using 4.00 g pluronic P123 (Mn = 5,800), 6.8 mL tetraethyl orthosilicate, 90.0 mL hydrochloric acid (2 M) and 21.0 mL deionized water. The mixture was transferred into the 100 mL-TEFLON lined autoclave; and kept in an oven at 100°C for 24 h. Then, the product was cooled to room temperature, filtered and washed with distilled water (100 mL) to remove residual surfactant and dried at room temperature. After that, the product was filtered and washed frequently with distilled water. After drying, the as-synthesized product was calcinated at 600°C for 6 h in order to remove the templates. In the next step, for synthesis of chlorinated SBA-15, 5.00 g of SBA-15 was stirred in dry toluene (50.0 mL) for 1 h. Then,

5.0 mL (20.76 mmol) of chloropropyltrimethoxysilane (CPTES) was added and refluxed at 122°C for 24 h under nitrogen atmosphere. The product was filtered, washed with toluene and ethanol (three times and each time with 30.0 mL of toluene and ethanol) and dried at 110°C for 4 h in a vacuum oven. Thereafter, a mixture of SBA-15-Cl (2.00 g), 2,4-dihydroxybenzaldehyde (2.83 g) and ethanolamine (2.00 g) in toluene (50.0 mL) were refluxed for 3 h. Then, the obtained solid named as SBA-15-HESI was filtered, washed by ethanol (96%) and dried in a vacuum oven at 80°C for 10 h. In this case, 0.10 g of mesoporous SBA-15-HESI was dispersed in 10.0 mL absolute ethanol solution. Then 1.0 mL of Fe₃O₄ nanoparticle suspension (32.2 mg L⁻¹) was added to the above solution and the mixture was agitated at room temperature for 18 h. The reaction mixture was deposited by magnet and washed several times with ethanol and distilled water. Finally, the brown colored product (SBA-15-HESI-Fe₃O₄) was dried at room temperature. All the steps of adsorbent preparation are shown in Fig. S1.

2.3. Ultrasonic-assisted MB adsorption experiments

The efficiency of MB removal was determined at different experimental conditions optimized according to the CCD method. The experiments were done in the range of 10–30 mg L⁻¹ of initial dye concentration. The stock solution of MB was prepared by dissolving solid dye in double-distilled water in laboratory flasks and the working concentrations were prepared daily by its suitable dilution. After setting pH and the adsorbent dose, the solution was kept in an ultrasonic bath for appropriate times, according to Table S1. At the end of the adsorption experiments, the sample was immediately separated with magnet easily and analyzed with UV–Vis spectrophotometer. The adsorbent capacity (q_e) was calculated using Eq. (1).

$$q_e = \frac{(C_0 - C_e)V}{m} \quad (1)$$

where C_0 and C_e (mg L⁻¹) are the initial and equilibrium dye concentration in aqueous solution, respectively. V (L) is the volume of dye solution and m (g) is the amount of the adsorbent [30].

2.4. Experimental design

In general, experimental design is used in order to optimize the important variables in a process as well as to minimize the number of experiments and to reduce the experimental error [14,31,32]. CCD, as a mathematical tool, is commonly applied to identify the significance of the effects of variables [18,33]. In this project, the effect of four factors including pH, initial dye concentration, amount of adsorbent and sonication time on adsorption efficiency was investigated. The software Design Expert 7.0.0 was used to designate the runs and further analysis of the data. Five levels of CCD were shown in Table 1. The total experiments were performed in 30 runs and 3 blocks (Table S1). The number of experiments was calculated using the following equation:

$$N_{\text{tot}} = 2^f + 2f + C_p \quad (2)$$

Table 1
Experimental parameters and levels in the central composite design

Factors	Levels				
	$-\alpha$	-1	0	+1	$+\alpha$
(A) Adsorbent dose (mg)	10	5	15	20	25
(B) pH	6	7	8	9	10
(C) Initial ion concentration (mg L ⁻¹)	10	15	20	25	30
(D) Sonicating time (min)	1	2	3	4	5

where N_{tot} is the total number of experiments, f shows the number of parameters and C_p is the center points [14,34].

Response surface methodology (RSM), a combination of mathematical and statistical techniques, was applied to develop, improve and optimize the adsorption process as well as evaluation of the significance and interaction of all corresponding factors [14,35–37]. The RSM modeling is on the basis of first or second-order polynomial equations followed by analysis of variance (ANOVA). Table S2 shows ANOVA data obtained by the experiments. The validated model plotted in tridimensional graph includes a surface response corresponding to the interaction between variables.

3. Results and discussion

3.1. Characterization of SBA-15-HESI-Fe₃O₄

IR spectrum of SBA-15, SBA-15-Cl, SBA-15-HESI, SBA-15-HESI-Fe₃O₄ and Fe₃O₄ is shown in Fig. S2(a). Fe₃O₄ IR spectrum revealed a broad peak at about 3,365 cm⁻¹ which is attributed to O–H stretching mode of water adsorbed from air. The vibration peak for Fe–O band was observed at 560 cm⁻¹. SBA-15, SBA-15-Cl, SBA-15-HESI and SBA-15-HESI-Fe₃O₄ exhibit a broad band at 3,000–3,500 cm⁻¹ corresponds to the O–H bond stretching of surface silanol groups. The peaks located at 1,089, 808 and 465 cm⁻¹ are belonging to the stretching and bending vibration of O–Si–O and Si–O of silanol groups band from SBA-15, respectively. After functionalization with CPTES, the vibration peaks of C–H in propyl group merged at 2,929 cm⁻¹ and stretching vibration of C–Cl cm⁻¹ band was also observed at 709 cm⁻¹. Furthermore, the peak at 1,643 cm⁻¹ is related to C=N stretching in HESI. It is important to imply that C–Cl stretching band was disappeared after reaction with N–H in HESI which indicates SBA-15-Cl has been successfully functionalized with HESI. For SBA-15-HESI-Fe₃O₄, the peak at 590 cm⁻¹ which belongs to Fe–O group confirms the formation of SBA-15-HESI-Fe₃O₄ nanocomposite.

Low-angle powder X-ray diffraction pattern of SBA-15, SBA-15-HESI and SBA-15-HESI-Fe₃O₄ (Fig. S2(b)) exhibited two weak peaks (110 and 200) and a single strong peak (100) in $2\theta = 0.6, 1.0$ and 1.9 , respectively, verifying the hexagonal structure of the synthesized materials and their good stability after each functionalization step. From XRD pattern of Fe₃O₄ nanoparticles (inset in Fig. S2(b)), eight characteristic peaks of Fe₃O₄ ($2\theta = 23.2, 27, 30.1, 35.4, 43.0, 44.5, 53.5$ and 57.0) are similar to those reported in literature.

According to the saturation magnetization curve (Fig. S2(c)), it is obvious that there is no hysteresis in the magnetization sweep. Therefore, the magnetic coercivity of the nanostructures is low and suggests the presence of Fe₃O₄ as superparamagnetic.

The shape and surface morphology of the samples (Fig. S3) were investigated by SEM and transmission electron microscopy (TEM) analysis. It can be seen that SBA-15 and SBA-15-HESI have regular morphology and ordered structure while changing the morphology of SBA-15-HESI after formation, the nanocomposite with Fe₃O₄ nanoparticles reflects the successful modification.

The N₂ adsorption–desorption isotherms of SBA-15, SBA-15-HESI and SBA-15-HESI-Fe₃O₄ obtained at 77k are shown in Fig. S4. Type IV isotherms, IUPAC adsorption–desorption isotherms, with H1-type hysteresis loops are obtained in samples, in a good agreement with the defined behavior of SBA-15. Some textural and physicochemical properties of SBA-15, SBA-15-HESI and SBA-15-HESI-Fe₃O₄ such as pore diameter (D_{BET}), the BET surface area, total pore volume (V_{total}) are given in Table S3 and Fig. S4. A considerable decrease in the BET surface area upon grafting of Fe₃O₄ nanoparticles at the surface of the functionalized SBA-15 material clearly suggests that the Fe₃O₄ nanoparticles have been anchored on the inner surface of the mesoporous material and some pore mouths have been partially blocked by the Fe₃O₄ nanoparticles.

3.2. Central composite design

The experiments in CCD were planned randomized to minimize the effect of uncontrolled factors [14,38]. As shown in Table 1, four factors adsorbent dose (A), pH (B), dye concentration (C) and sonication time (D) were planned in three (low, center and high) as coded values ($-\alpha, 0, +\alpha$). All 30 experiments with condition of each parameters are listed in Table S1. The last column reveals response in terms of adsorption capacity of the adsorbent under the related situation.

In order to find out the most effective factors and their interaction, analysis of variance (ANOVA) was evaluated. According to the literature, the p values less than 0.05 in ANOVA table indicate the statistical significance of an effect at 95% confidence level. F -test was used to estimate the statistical significance of all terms in the polynomial equation within 95% confidence interval. Sum of squares shows that adsorbent dosage has maximum effect on adsorption. Moreover, the most interaction occurs between dye concentration and adsorbent dosage. Data analysis gave the following equation for removal of MB by the synthesized adsorbent:

$$\begin{aligned}
 R1 = & +50.30 - 22.61A + 2.27B + 15.89C + 0.14D \\
 & - 0.80AB - 4.65AC - 0.040AD + 1.44BC \\
 & + 0.023BD - 0.21CD + 5.34A^2 - 0.54B^2 \\
 & - 0.41C^2 - 0.14D^2
 \end{aligned} \quad (3)$$

3.3. Response surface methodology

RSM was developed in the next step to optimize the important parameters and describe the nature of the response surface in the experiment [13,39]. Fig. 1 displays the

three-dimensional plots of variables including the response surface plots of adsorption capacity vs. significant variables obtained for a given pair of factors at fixed and optimal values of other variables. The curvatures of these plots

indicate the significant interaction between the parameters [40]. Figs. 1(a)–(f) reveal the interaction of paired parameters with each other. As shows in Fig. 1(a) maximum adsorbent capacity occurs in low adsorbent dose and high time that is

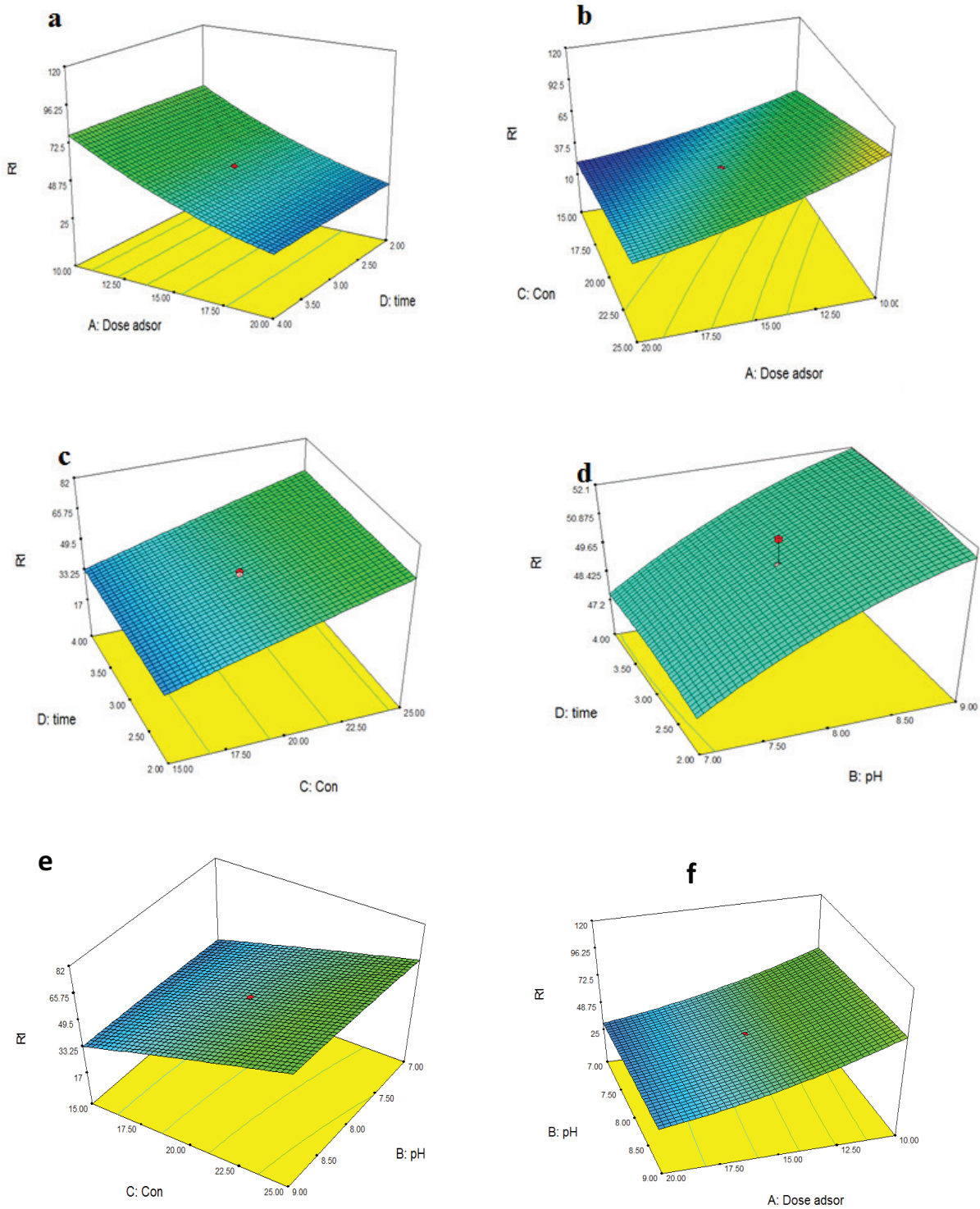


Fig. 1. Three-dimensional plots of R_{MB} (a) adsorbent dose and time, (b) adsorbent dose and MB concentration, (c) MB concentration and time, (d) time and pH, (e) MB concentration and pH, (f) adsorbent dose and pH, while other parameters were kept at their optimum values.

the result of the time of contacting adsorbent and dye increase. As Fig. 1(b) shows, for having high adsorbent capacity, lower adsorbent dose and higher dye concentration are needed and this concept is in fit with Eq. (1). Fig. 1(c) gives the interaction of time and dye concentration. To obtain maximum response, it is better that adsorption is done at higher dye concentration and lower time. Adsorbent capacity has direct relation with dye concentration according to Eq. (1). Time has no important role in increasing adsorbent capacity according to Figs. 1(a) and (c) and it is considered that the adsorption rate is very fast and time factor is not an effective parameter for MB removal. This even may be attributed to the high available surface area and active sites of adsorbent. However, the important role of ultrasonic power on improvement of the mass transfer process via amplifying the affinity between adsorbate and adsorbent and accelerating the chemical process cannot be ignored.

The increase in adsorption capacity at higher pH values was observed which may be attributed to the increase in electrostatic attraction between cationic dye molecule and active sites of the sorbent followed by higher dye uptake on the adsorbent surface. Furthermore, it was found that maximum adsorption capacity occurred in low adsorbent dose which is in agreement with Eq. (1). As shown in Fig. 2, the plot of experimental values of adsorbent capacity vs. those calculated from Eq. (3) indicated a good fit.

3.4. Adsorption equilibrium study

The data obtained by the current study were fitted to various adsorption isotherm equation such as Langmuir, Freundlich and Temkin [18,41]. The concentration of dye solution for adsorption equilibrium study was in the range of 10–90 mg L⁻¹. The constant parameters and correlation coefficient (R^2) obtained from the plots of known equation for Langmuir, Freundlich and Temkin are shown in Table 2. The plots of corresponding isotherms are also shown in Fig. S5.

Based on the linear form of Langmuir isotherm model and its higher value of R^2 , isotherm of the proposed adsorption processes efficiently followed Langmuir equation.

3.5. Adsorption kinetic modeling

The kinetics of adsorption is necessary for industrial applications. The experimental kinetic data of MB removal were considered by conventional models including pseudo-first-order and pseudo-second-order [42]. The constants of each models are summarized in Table 3.

The values of R^2 indicate the tendency of data to agree with pseudo-second-order kinetic model. Fig. S6 shows the kinetic models.

3.6. Recovery and reusability

The good reusability is a main factor for an ideal adsorbent [42]. In this study, recovery of the adsorbent was performed by HCl and NaOH 0.1 M solutions. After five consecutive cycles, the adsorption capacity of the adsorbent still remained above 90%. The amount of adsorption capacity in each cycle is depicted in Table 4.

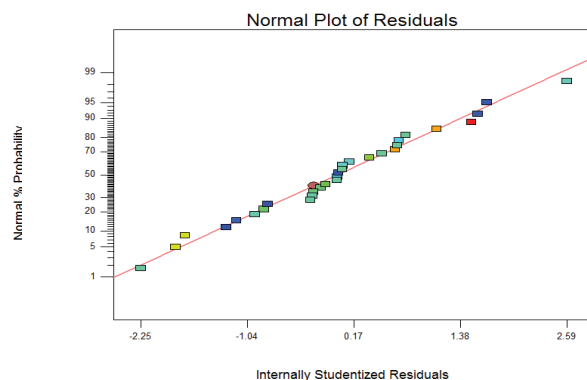


Fig. 2. The experimental data vs. the predicted data of normalized removal of MB.

Table 2
Adsorption isotherms of MB adsorption onto SBA-15-HESI-Fe₃O₄

Isotherm	Equation	Parameter	Values of parameters MB
Langmuir	$\frac{C_e}{q_e} = \frac{C_e}{q_m} + \frac{1}{K_L q_m}$	q_m	181.81
		K_L	
		R^2	0.97
Freundlich	$\ln q_e = \ln K_F + \frac{1}{n} \ln C_e$	K_F	
		n	3.04
		R^2	0.61
Temkin	$q_e = B_1 \ln K_T + B_1 \ln C_e$	K_T	
		B_1	72.01
		R^2	0.79

Table 3
Pseudo-first-order and pseudo-second-order kinetic constants of MB adsorption onto SBA-15-HESI-Fe₃O₄

Model	Equation	Parameters	Values of parameters MB
First-order	$\log(q_e - q_t) = \log q_{e1} - \frac{k_1}{2.303} t$	q_e (mg g ⁻¹)	2.656
		K_1 (L min ⁻¹)	0.6031
		R^2	0.9837
Second-order	$\frac{t}{q_t} = \frac{1}{k_2 q_{e2}^2} + \frac{1}{q_{e2}} t$	K_2 (g mg ⁻¹ min ⁻¹)	0.150417
		q_{e2}	105.26
		R^2	1.0000

It is important to investigate the efficiency of adsorbent on the real samples, because of the heterogeneity and complexity of these samples compared with the model samples prepared in laboratory. For confirming the applicability of the SBA-15-HESI-Fe₃O₄, two types of water samples were used including water from carpet cleaning and dyeing (Table 5).

A comparison between the performance of the proposed adsorbent and method with some adsorbents and methods is listed in Table 6.

4. Conclusion

In the current project, SBA-15-HESI-Fe₃O₄ was proposed as an efficient adsorbent for removal of MB from aqueous media. In most of the magnetic sorbents, the presence of magnetic component allows convenient magnetic separation rather than traditional filtration or centrifugation. On the other hand, SBA-15 has high hydrophobic mesoporous surface. The hydrophilic surface of Fe₃O₄ nanoparticles provides

unique environment for hydrophobic molecules uptake such as methylene blue cationic dye. Therefore, in this case SBA-15-HESI is seemed to be responsible for adsorption due to its high surface area. However, the iron oxide nanoparticles embedded in the SBA-15-HESI will enhance the adsorption capacity of the synthesized adsorbent. The optimum conditions (pH = 9, initial dye concentration = 25 mg L⁻¹, adsorbent dose = 10 mg and sonication time = 3.5 min) were determined by experimental design methodology. Ultrasound irradiation was used in order to accelerate the adsorption process. Ultrasonic power had important role in shortening the adsorption time of MB by enhancing the dispersion of adsorbent in solution. The equilibrium and kinetic studies were investigated under optimal condition obtained by response surface methodology. The experimental data were in agreement with Langmuir model. The experiments were done in optimum condition obtained by RSM except initial dye concentration. By using the Langmuir plot and Langmuir equation, the maximum adsorption capacity of the adsorbent obtained was 172.3 mg g⁻¹. The process kinetics can be successfully fitted to the pseudo-second-order kinetic model. The developed adsorbent provided many advantages in terms of high percentage removal, reusability under mild condition, stability and easy to synthesize. The performance of magnetic mesoporous silica adsorbent (SBA-15-HESI-Fe₃O₄) was examined on the real wastewaters samples and confirmed the applicability of magnetic adsorbent for practical applications.

Acknowledgments

The authors would like to thank Iran University of Science and Technology and also Iran Nanotechnology Initiative Council for financial support of the work.

References

- [1] J.W. Lee, S.P. Choi, R. Thiruvengatchari, W.G. Shim, H. Moon, Evaluation of the performance of adsorption and coagulation processes for the maximum removal of reactive dyes, *Dyes Pigm.*, 69 (2006) 196–203.
- [2] R. Ahmad, R. Kumar, Adsorption studies of hazardous malachite green onto treated ginger waste, *J. Environ. Manage.*, 91 (2010) 1032–1038.
- [3] F.N. Azad, M. Ghaedi, K. Dashtian, S. Hajati, A. Goudarzi, M. Jamshidi, Enhanced simultaneous removal of malachite green and safranin O by ZnO nanorod-loaded activated carbon: modeling, optimization and adsorption isotherms, *New J. Chem.*, 39 (2015) 7998–8005.
- [4] M.U. Naushad, Z.A. AL-Othman, M.R. Awual, S.M. Alfadul, T. Ahamad, Adsorption of rose Bengal dye from aqueous solution by amberlite Ira-938 resin: kinetics, isotherms, and thermodynamic studies, *Desal. Wat. Treat.*, 57 (2016) 13527–13533.
- [5] S.A. El-Safty, A. Shahat, M.R. Awual, Efficient adsorbents of nanoporous aluminosilicate monoliths for organic dyes from aqueous solution, *J. Colloid Interface Sci.*, 359 (2011) 9–18.
- [6] R.H. Schirmer, H. Adlra, M. Pickhardt, E. Mandelkow, Lest we forget you methylene blue, *Neurobiol. Aging*, 32 (2011) 2325. e7–2325.e16.
- [7] D.W. O'Connell, C. Birkinshaw, T.F. O'Dwyer, Heavy metal adsorbents prepared from the modification of cellulose, *Bioresour. Technol.*, 99 (2008) 6709–6724.
- [8] S. Sun, H. Zeng, D.B. Robinson, S. Raoux, P.M. Rice, S.X. Wang, G. Li, Monodisperse MFe₂O₄ (M = Fe, Co, Mn) nanoparticles, *J. Am. Chem. Soc.*, 126 (2004) 273–279.

Table 4

Regeneration process parameters of five adsorption/desorption cycles

Dye	Cycle no.	$q_{c,exp}$ (mg g ⁻¹)	% Removal
MB	1	100.41	97.18
	2	104.67	95.02
	3	102.34	93.63
	4	102.82	91.83
	5	103.50	90.64

Table 5

Results of real samples analysis for adsorption of MB (25 ppm) over the SBA-15-HESI-Fe₃O₄

Sample	Adsorption capacity (mg g ⁻¹)	R.S.D. %
Carpet cleaning wastewater	90.27	1.46
Dyeing wastewater	88.66	1.35

Table 6

Comparison for the removal of MB dyes by different adsorbents and methods

Adsorbent	Dye	Concentration (mg L ⁻¹)	Contact time (min)	q^a (mg g ⁻¹)	Refs.
Activated carbon	MB	100	30	64.30	[43]
Zeolite	MB	230	840	22.0	[44]
Ag-NP-AC	MB	20	10	71.4	[45]
HKUST-1 (Cu-BTC)	MB	3.2	20–360	4.88	[46]
SBA-15-HESI-Fe ₃ O ₄	MB	25	3.5	172.3	This study

^aAdsorption capacity.

- [9] Y. Bulut, Z. Tez, Removal of heavy metals from aqueous solution by sawdust adsorption, *J. Environ. Sci.*, 19 (2007) 160–166.
- [10] M.B. Tabacco, T.G. DiGiuseppe, Optical chemical sensors for environmental control and system management, *Adv. Space Res.*, 18 (1996) 125–134.
- [11] H. Mazaheri, M. Ghaedi, S. Hajati, K. Dashtian, M. Purkait, Simultaneous removal of methylene blue and Pb^{2+} ions using ruthenium nanoparticle-loaded activated carbon: response surface methodology, *RSC Adv.*, 5 (2015) 83427–83435.
- [12] M. Ghaedi, S. Hajati, M. Zare, M. Zare, S.S. Jaber, Experimental design for simultaneous analysis of malachite green and methylene blue; derivative spectrophotometry and principal component-artificial neural network, *RSC Adv.*, 5 (2015) 38939–38947.
- [13] M.S. Tehrani, R. Zare-Dorabei, Competitive removal of hazardous dyes from aqueous solution by MIL-68(Al): derivative spectrophotometric method and response surface methodology approach, *Spectrochim. Acta, Part A*, 160 (2016) 8–18.
- [14] M.S. Tehrani, R. Zare-Dorabei, Highly efficient simultaneous ultrasonic-assisted adsorption of methylene blue and rhodamine B onto metal organic framework MIL-68(Al): central composite design optimization, *RSC Adv.*, 6 (2016) 27416–27425.
- [15] M. Namvari, H. Namazi, Synthesis of magnetic citric-acid-functionalized graphene oxide and its application in the removal of methylene blue from contaminated water, *Polym. Int.*, 63 (2014) 1881–1888.
- [16] A. Shahbazi, H. Younesi, A. Badiei, Functionalized SBA-15 mesoporous silica by melamine-based dendrimer amines for adsorptive characteristics of $Pb(II)$, $Cu(II)$ and $Cd(II)$ heavy metal ions in batch and fixed bed column, *Chem. Eng. J.*, 168 (2011) 505–518.
- [17] C. Yuwei, W. Jianlong, Preparation and characterization of magnetic chitosan nanoparticles and its application for $Cu(II)$ removal, *Chem. Eng. J.*, 168 (2011) 286–292.
- [18] R. Zare-Dorabei, V. Jalalat, A. Tadjarodi, Central composite design optimization of $Ce(III)$ ion removal from aqueous solution using modified SBA-15 mesoporous silica, *New J. Chem.*, 40 (2016) 5128–5134.
- [19] S. Dashamiri, M. Ghaedi, K. Dashtian, M.R. Rahimi, A. Goudarzi, R. Jannesar, Ultrasonic enhancement of the simultaneous removal of quaternary toxic organic dyes by CuO nanoparticles loaded on activated carbon: central composite design, kinetic and isotherm study, *Ultrason. Sonochem.*, 31 (2016) 546–557.
- [20] M.R. Awual, M.M. Hasan, T. Ihara, T. Yaita, Mesoporous silica based novel conjugate adsorbent for efficient selenium(IV) detection and removal from water, *Microporous Mesoporous Mater.*, 197 (2014) 331–338.
- [21] M.R. Awual, T. Yaita, S.A. El-Safty, H. Shiwaku, Y. Okamoto, S. Suzuki, Investigation of palladium(II) detection and recovery using ligand modified conjugate adsorbent, *Chem. Eng. J.*, 222 (2013) 172–179.
- [22] M.R. Awual, M.M. Hasan, A novel fine-tuning mesoporous adsorbent for simultaneous lead(II) detection and removal from wastewater, *Sens. Actuators, B*, 202 (2014) 395–403.
- [23] A. Kavosi, F. Faridbod, M.R. Ganjali, Solid phase extraction of some lanthanide ions by functionalized SBA-15 from environmental samples, *Int. J. Environ. Res.*, 9 (2015) 247–254.
- [24] L. Hajiaghababaei, B. Ghasemi, A. Badiei, H. Goldooz, M.R. Ganjali, G. Mohammadi Ziarani, Aminobenzenesulfonamide functionalized SBA-15 nanoporous molecular sieve: a new and promising adsorbent for preconcentration of lead and copper ions, *J. Environ. Sci.*, 24 (2012) 1347–1354.
- [25] A. Tadjarodi, V. Jalalat, R. Zare-Dorabei, Adsorption of $La(III)$ in aqueous systems by N-(2-hydroxyethyl) salicylaldehyde-functionalized mesoporous silica, *Mater. Res. Bull.*, 61 (2015) 113–119.
- [26] J.P.S. Fernandes, B.S. Carvalho, C.V. Luhez, M.J. Politi, C.A. Brandt, Optimization of the ultrasound-assisted synthesis of allyl 1-naphthyl ether using response surface methodology, *Ultrason. Sonochem.*, 18 (2011) 489–493.
- [27] A. Keramat, R. Zare-Dorabei, Ultrasound-assisted dispersive magnetic solid phase extraction for preconcentration and determination of trace amount of $Hg(II)$ ions from food samples and aqueous solution by magnetic graphene oxide: central composite design optimization, *Ultrason. Sonochem.*, 38 (2017) 421–429.
- [28] M. Roosta, M. Ghaedi, A. Asfaram, Simultaneous ultrasonic-assisted removal of malachite green and safranin O by copper nanowires loaded on activated carbon: central composite design optimization, *RSC Adv.*, 5 (2015) 57021–57029.
- [29] R. Zare-Dorabei, S.M. Ferdowsi, A. Barzin, A. Tadjarodi, Highly efficient simultaneous ultrasonic-assisted adsorption of $Pb(II)$, $Cd(II)$, $Ni(II)$ and $Cu(II)$ ions from aqueous solutions by graphene oxide modified with 2,2'-dipyridylamine: central composite design optimization, *Ultrason. Sonochem.*, 32 (2016) 265–276.
- [30] W. Yantasee, C.L. Warner, T. Sangvanich, R.S. Addleman, T.G. Carter, R.J. Wiacek, G.E. Fryxell, C. Timchalk, M.G. Warner, Removal of heavy metals from aqueous systems with thiol functionalized superparamagnetic nanoparticles, *Environ. Sci. Technol.*, 41 (2007) 5114–5119.
- [31] M.A. Bezerra, R.E. Santelli, E.P. Oliveira, L.S. Villar, L.A. Escalera, Response surface methodology (RSM) as a tool for optimization in analytical chemistry, *Talanta*, 76 (2008) 965–977.
- [32] H. Ebrahimi-Najafabadi, R. Leardi, M. Jalali-Heravi, Experimental design in analytical chemistry – part II: applications, *J. AOAC Int.*, 97 (2014) 12–18.
- [33] F.M. Pang, S.P. Teng, T.T. Teng, A. Omar, Heavy metals removal by hydroxide precipitation and coagulation-flocculation methods from aqueous solutions, *Water Qual. Res. J. Can.*, 44 (2009) 174–182.
- [34] M.M. Brbooti, B.A. Abid, N.M. Al-Shuwaiki, Removal of heavy metals using chemical precipitation, *Eng. Technol. J.*, 29 (2011) 595–612.
- [35] E. Martendal, D. Budziak, E. Carasek, Application of fractional factorial experimental and Box-Behnken designs for optimization of single-drop microextraction of 2,4,6-trichloroanisole and 2,4,6-tribromoanisole from wine samples, *J. Chromatogr. A*, 1148 (2007) 131–136.
- [36] S.N. Deming, S.L. Morgan, *Experimental Design: A Chemometric Approach*, Elsevier, Vol. 11, 1993, 436 p.
- [37] S. Huang, C. Li, Z. Cheng, Y. Fan, P. Yang, C. Zhang, K. Yang, J. Lin, Magnetic Fe_3O_4 @mesoporous silica composites for drug delivery and bioadsorption, *J. Colloid Interface Sci.*, 376 (2012) 312–321.
- [38] M. Tjernström, C. Leck, C.E. Birch, J.W. Bottenheim, B.J. Brooks, I.M. Brooks, L. Bäcklin, R.Y.-W. Chang, G. de Leeuw, L. Di Liberto, S. de la Rosa, E. Granath, M. Graus, A. Hansel, J. Heintzenberg, A. Held, A. Hind, P. Johnston, J. Knulst, M. Martin, P.A. Matrai, T. Mauritsen, M. Müller, S.J. Norris, M.V. Orellana, D.A. Orsini, J. Paatero, P.O.G. Persson, Q. Gao, C. Rauschenberg, Z. Ristovski, J. Sedlar, M.D. Shupe, B. Sierau, A. Sirevaag, S. Sjogren, O. Stetzer, E. Swietlicki, M. Szczodrak, P. Vaattovaara, N. Wahlberg, M. Westberg, C.R. Wheeler, The Arctic Summer Cloud Ocean Study (ASCOS): overview and experimental design, *Atmos. Chem. Phys.*, 14 (2014) 2823–2869.
- [39] F. Taghizadeh, M. Ghaedi, K. Kamali, E. Sharifpour, R. Sahraie, M.K. Purkait, Comparison of nickel and/or zinc selenide nanoparticle loaded on activated carbon as efficient adsorbents for kinetic and equilibrium study of removal of Arsenazo (III) dye, *Powder Technol.*, 245 (2013) 217–226.
- [40] H. Ebrahimi-Najafabadi, R. Leardi, M. Jalali-Heravi, Experimental design in analytical chemistry – part I: theory, *J. AOAC Int.*, 97 (2014) 3–11.
- [41] M. Noori Sepehr, H. Kazemian, E. Ghahramani, A. Amrane, V. Sivasankar, M. Zarrabi, Defluorination of water via Light Weight Expanded Clay Aggregate (LECA): adsorbent characterization, competing ions, chemical regeneration, equilibrium and kinetic modeling, *J. Taiwan Inst. Chem. Eng.*, 45 (2014) 1821–1834.
- [42] D. Oke, S. Ndlovu, V. Sibanda, Removal of platinum group metals from dilute process streams: identification of influential factors using DOE approach, *J. Environ. Chem. Eng.*, 2 (2014) 1061–1069.

- [43] C.S. Ozdemir, Adsorption and desorption kinetics behavior of methylene blue onto activated carbon, *Physicochem. Prob. Miner. Process.*, 48 (2012) 441–454.
- [44] R. Han, J. Zhang, P. Han, Y. Wang, Z. Zhao, M. Tang, Study of equilibrium, kinetic and thermodynamic parameters about methylene blue adsorption onto natural zeolite, *Chem. Eng. J.*, 145 (2009) 496–504.
- [45] M. Ghaedi, Sh. Heidarpour, S.N. Kokhdan, R. Sahraie, A. Daneshfar, B. Brazesh, Comparison of silver and palladium nanoparticles loaded on activated carbon for efficient removal of Methylene blue: kinetic and isotherm study of removal process, *Powder Technol.*, 228 (2012) 18–25.
- [46] S. Lin, Z. Song, G. Che, A. Ren, P. Li, C. Liu, J. Zhang, Adsorption behavior of metal–organic frameworks for methylene blue from aqueous solution, *Microporous Mesoporous Mater.*, 193 (2014) 27–34.

Supplementary materials

Table S1
The design matrix for four variables with adsorption capacity (mg g⁻¹) for MB as response (R)

Run	Block	A	B	C	D	Response (R)
1	1	10	7	15	4	54.4
2	1	20	9	15	4	22.57
3	1	15	8	20	3	49.13
4	1	15	8	20	3	51.2
5	1	20	7	15	2	18.125
6	1	10	9	15	2	56.12
7	1	20	7	25	4	40.47
8	1	20	9	25	2	45.75
9	1	10	9	25	4	103.1
10	1	10	7	25	2	90.35
11	2	15	8	20	3	50.1
12	2	10	9	15	4	58.3
13	2	20	7	25	2	40.22
14	2	20	7	15	4	19.75
15	2	10	7	15	2	54.2
16	2	10	9	25	2	102.9
17	2	20	9	25	4	45.92
18	2	10	7	25	4	90.55
19	2	20	9	15	2	22.47
20	2	15	8	20	3	51.1
21	3	15	8	10	3	17.6
22	3	15	8	20	5	50.33
23	3	15	10	20	3	50.43
24	3	15	8	20	1	51.06
25	3	15	8	30	3	81.63
26	3	15	6	20	3	47.76
27	3	15	8	20	1	25.64
28	3	15	8	20	3	51.1
29	3	15	8	20	3	49.16
30	3	5	8	20	3	119.6

Table S2
Analysis of variance (ANOVA) for the model applied for MB adsorption by SBA-15-HESI-Fe₃O₄

Source	Sum of squares	df	Mean square	F-value	<i>p</i> value	
Block	8.91	2	4.46			
Model	19,711.19	14	1,407.94	282.25	<0.0001	Significant
A-Dose of adsorbent	12,265.70	1	12,265.70	2,458.94	<0.0001	
B-pH	123.33	1	123.33	24.72	0.0003	
C-Dye concentration	6,060.60	1	6,060.60	1,214.98	<0.0001	
D-Sonication time	0.50	1	0.50	0.10	0.7565	
AB	10.20	1	10.20	2.04	0.1763	
AC	364.29	1	364.29	69.42	<0.0001	
AD	0.025	1	0.025	5.052E-003	0.9444	
BC	33.34	1	33.34	6.68	0.0226	
BD	8.789E-003	1	8.789E-003	1.762E-003	0.9672	
CD	0.67	1	0.67	0.14	0.719	
A ²	782.68	1	782.68	156.91	<0.0001	
B ²	7.98	1	7.98	1.60	0.2281	
C ²	4.60	1	4.60	0.92	0.3545	
D ²	0.53	1	0.53	0.11	0.7489	
Residual	64.85	13	4.99			
Lack of fit	60.32	10	6.03	4	0.1405	Not significant
Pure error	4.52	3	1.51			
Corrected total	19,784.95	29				

Table S3
BET and BJH data of SBA-15, SBA-HESI and Fe₃O₄-SBA-HESI

Sample	BET surface area (m ² g ⁻¹)	Pore diameter (BJH) (Å)	Total pore volume (m ³ g ⁻¹)
SBA-15	869	85	1.034
SBA-15 HESI	234	64	0.399
Fe ₃ O ₄ -SBA-15 HESI	197	55	0.396

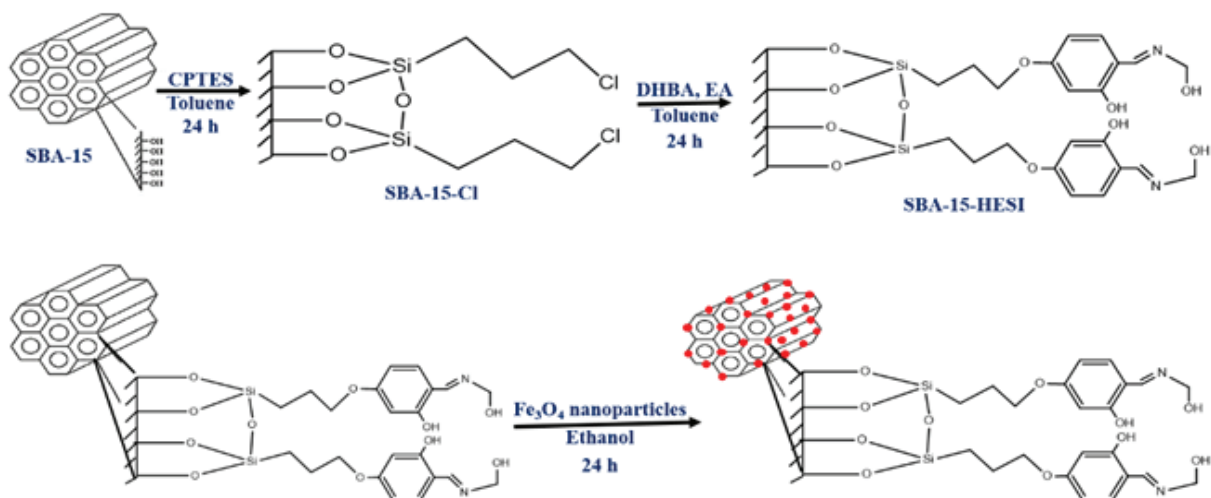
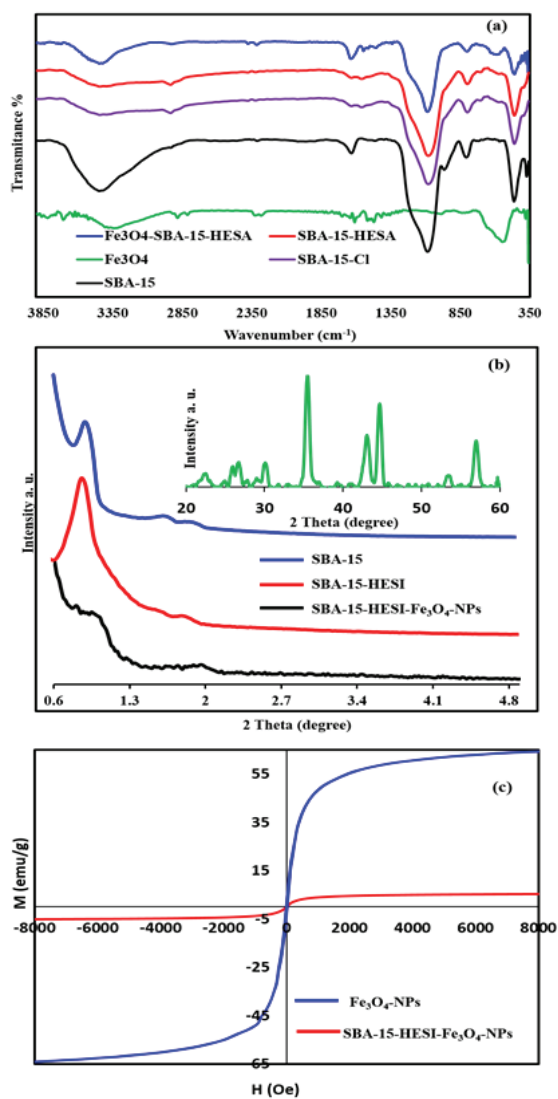
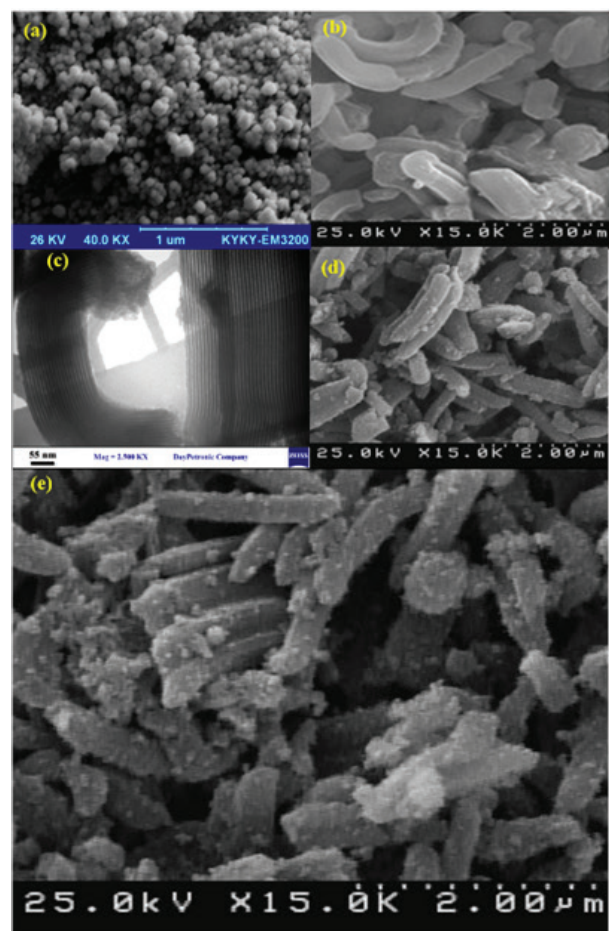
Fig. S1. Steps for the synthesis of SBA-15-HESI-Fe₃O₄.

Fig. S2. (a) FT-IR spectrum, (b) low-angle XRD of all samples and (c) vibrating sample magnetometer of magnetite samples.

Fig. S3. SEM images for Fe₃O₄ nanoparticles (a) and SBA-15 (b). TEM image of SBA-15 (c) and SEM images of SBA-15-HESI (d) and Fe₃O₄-SBA-15-HESI (e).

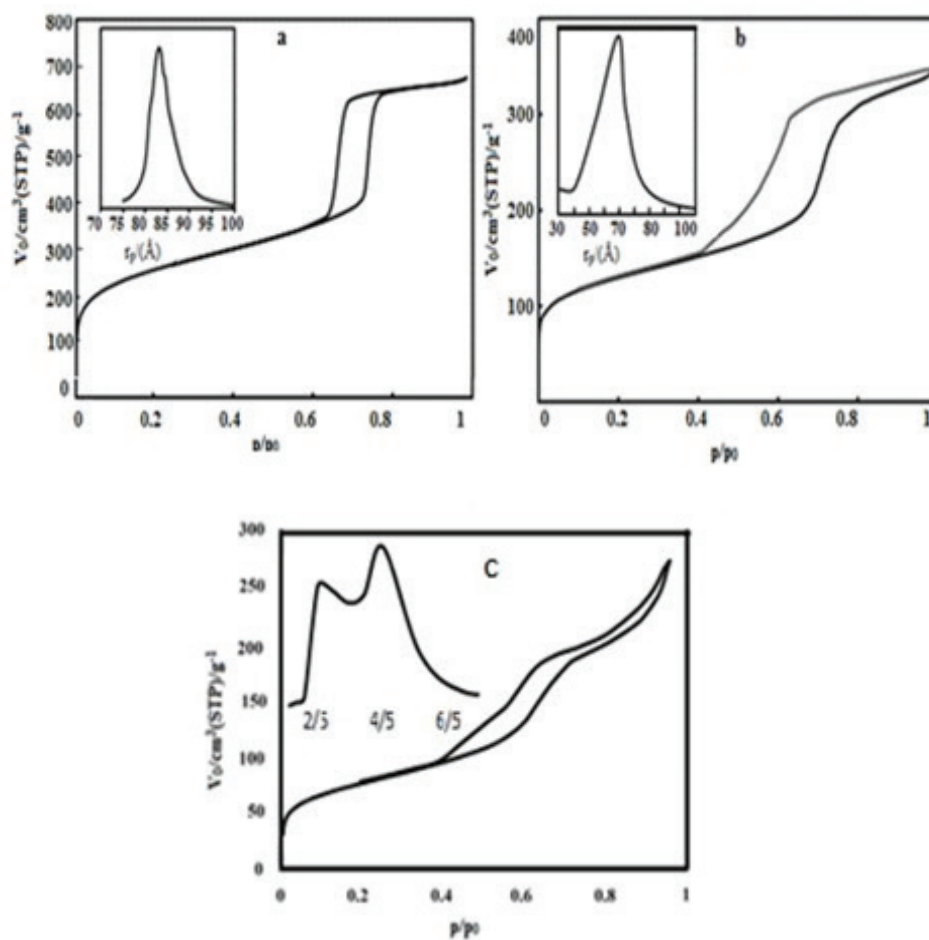


Fig. S4. Nitrogen adsorption–desorption isotherms (BET) for SBA-15 (a), SBA-HESI (b) and Fe_3O_4 -SBA-HESI (c).

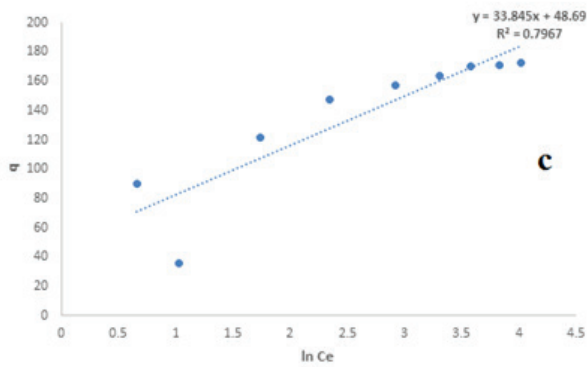
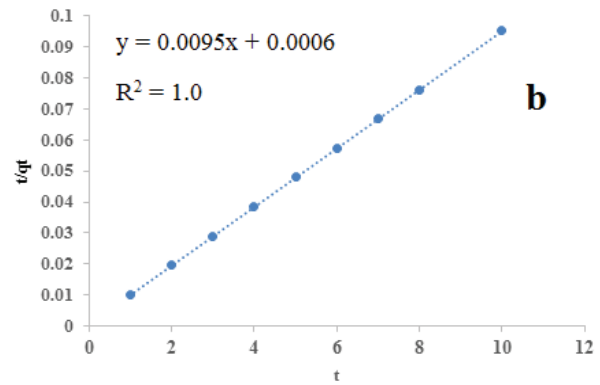
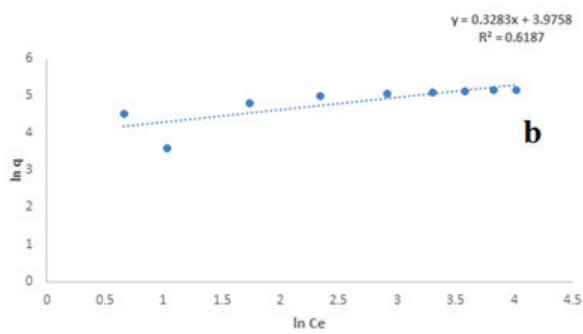
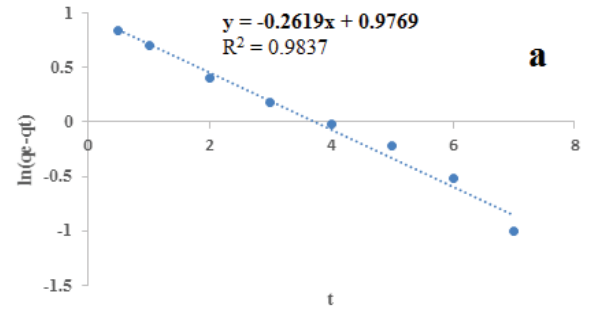
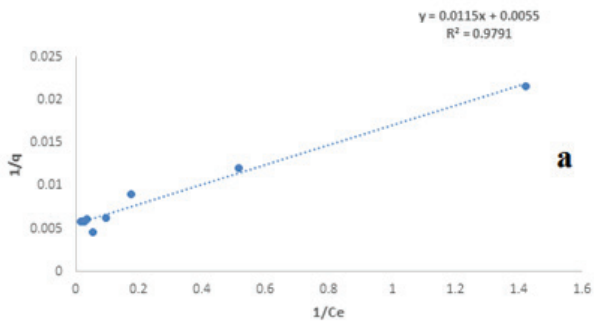


Fig. S6. The plots of pseudo-first-order (a) and pseudo-second-order (b) models.

Fig. S5. Langmuir (a), Freundlich (b) and Temkin (c) isotherms.